Insertion and diffusion of N and C in γ –TiAl: Theoretical study and comparison with O

Enrica Epifano, Gilles Hug, Damien Connétable

Journal Pre-proof

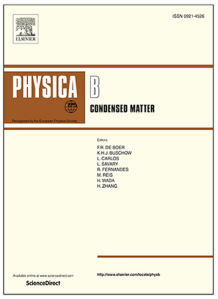

Insertion and diffusion of N and C in γ–TiAl: Theoretical study and comparison with O

E. Epifano, G. Hug, D. Connétable

PII: S0921-4526(21)00537-8
DOI: https://doi.org/10.1016/j.physb.2021.413370
Reference: PHYSB 413370

To appear in: *Physica B: Physics of Condensed Matter*

Received date : 12 November 2020
Revised date : 7 July 2021
Accepted date : 27 August 2021

Please cite this article as: E. Epifano, G. Hug and D. Connétable, Insertion and diffusion of N and C in γ–TiAl: Theoretical study and comparison with O, *Physica B: Physics of Condensed Matter* (2021), doi: https://doi.org/10.1016/j.physb.2021.413370.

Insertion and diffusion of N and C in γ–TiAl: theoretical study and comparison with O

E. Epifano[a,b], G. Hug[a], D. Connétable[b]

[a]*Laboratoire d'Etudes des Microstructures, CNRS-ONERA, Boite Postale 72, 92322 Châtillon Cedex, France*
[b]*CIRIMAT, UMR 5085, CNRS INP UPS, ENSIACET 4, allee Emile Monso, BP 44362, F-31030 Toulouse, Cedex 4 France*

Abstract

Nitrogen and carbon play an important role in the oxidation of Ti-Al intermetallic alloys in air. The insertion and diffusion of these elements in the γ-TiAl phase are investigated by first-principle computations. The accommodation of C and N atoms in several likely interstitial positions has been evaluated using density functional theory (DFT) calculations. The results show that both carbon and nitrogen prefer Ti-rich environments. Then, considering the possible jumps among the stable and metastable interstitial sites, the diffusion coefficients have also been obtained from *ab initio* calculations. According to the Transitional State Theory, in order to compute atomic jump rates, diffusion energy barriers and vibrational modes need to be known. Herein, barrier energies are obtained using the Climbing Image Nudged Elastic Band method. Vibrational properties are computed using the finite displacement method. Finally, diffusion coefficients are obtained solving the transport equation in the infinite time limit, using an analytical approach. The obtained results are compared to the diffusion of oxygen in γ-TiAl, investigated in previous studies. An anisotropic diffusion is obtained for all the interstitial species.

1. Introduction

Titanium-aluminum intermetallic alloys combine low densities with good mechanical properties at high temperatures [1, 2] and they are hence suitable for many applications in auto-mobile, marine and aerospatial industries. For instance, TiAl alloys are currently used for turbomachines in airplanes [3]. These alloys present generally two main intermetallic phases: α_2–Ti_3Al and γ–TiAl, with the latter being the most abundant one. However, the low oxidation resistance at high temperature is a limiting factor for the use of these materials. Indeed, even in the Al-richer γ–TiAl phase, the oxidation proceeds through a competitive formation of the passivating, desirable Al_2O_3 scale and the porous, deleterious TiO_2 rutile [4, 5, 6, 7].

Various works focused on understanding and improving the oxidation resistance of γ-TiAl based alloys [8, 9, 10, 11, 12, 13, 14, 15, 16, 17, 18, 19, 20]. Both internal and external oxidation generally occur [5, 21] in these materials. External oxidation results from the outward diffusion of Ti and Al species, while the internal one is due to the inward diffusion of oxygen. Therefore, in order to predict the evolution of oxidation reactions in these materials, one needs to know the diffusion coefficients of all the involved species, i.e. the metallic species of the alloy and the light atoms coming from the atmosphere. Measurements of the Al and Ti self-diffusion coefficients in γ-TiAl are available in the literature [22, 23, 24], but no experimental data exist for the diffusion of light interstitial atoms-such as oxygen, carbon and nitrogen- in γ-TiAl. Nevertheless, for oxygen, some data have been recently provided using *ab initio* calculations [25, 26, 27] and the proposed values agree quite well one with the other. In particular, all the three works reported an anisotropic diffusion of oxygen in γ-TiAl: the diffusion coefficients are equal in the x and y directions, while lower values are found along the z direction. The diffusion coefficients of C and N atoms are also necessary to fully understand oxidation in these materials. Indeed, various studies have highlighted that the oxidation of TiAl-based alloys is different in air and pure oxygen [5]. This indicates that N and C play an important role. In particular, the precipitation of nitrides (mostly TiN and Ti_2AlN) has been reported several times for oxidation in air [5, 6, 4, 7, 8]. In order to fill the gap existing in the literature, diffusion coefficients for nitrogen and carbon in stoichiometric γ-TiAl are herein obtain from first-principle calculations. On the atomic scale, the fundamental quantities to be determined in order to obtain the diffusion coefficients are the atomic jumping rates of the diffusing

species. In this work, the possible interstitial sites in which N and C can be accommodated are determined by Density Functional Theory (DFT). Then, the barrier energies to overcome to jump from one site to another are obtained from Climbing Image Nudge Elastic Band (CI-NEB) calculations. Combining these results with phonon calculations, the jumping rates are computed, according to the transitional state theory [28]. Finally, the diffusion coefficients are determined using an analytical Multi-State Diffusion method [29, 30]. This theoretical approach has already been applied to obtain diffusion coefficients of various light, interstitial atoms in monoatomic metals, such as aluminium [31], titanium [32, 33, 34] and nickel [35, 31], and for the diffusion of hydrogen [36], boron [26] and oxygen [26, 27] in γ-TiAl. The comparison with the experimental data, when available, has generally given a fair agreement, validating the computational approach.

The rest of this work is divided as following. In section 2, methods and calculation details are explained. In particular, in section 2.3, the crystallographic structure of γ-TiAl is shown and the choice of the tested interstitial positions is explained. In section 3, the calculation results are shown: first, the determination of the stable interstitial positions for C and N; second, the energy paths obtained from NEB; finally, the diffusion coefficients. In conclusion, the results obtained for C and N are discussed and compared to those previously reported for oxygen.

2. Methods

2.1. Theory

According to the Transitional State Theory of Eyring [28], the atomic jumping rate ν between two sites in a crystal is expressed by an Arrhenius equation:

$$\nu = \nu^* e^{-\Delta E/k_b T} \tag{1}$$

where k_B is the Boltzmann constant, T is the temperature, ν^* is a pre-factor generally called *attempt frequency* and ΔE is an activation energy barrier.

As all thermally activated processes, diffusion in crystals occurs following the Minimum Energy Path (MEP). In this study, the Climbing Image Nudged Elastic Band (CI-NEB), available within the VASP code [37, 38], has been used to find the MEP, the relative transitional state and hence the energy barrier ΔE. The prefactor ν^* is expressed as [28]:

$$\nu^* = \frac{k_B T}{h} \frac{Z_{ts}}{Z_{ie}} \tag{2}$$

where h is the Planck constant, Z_{ie} and Z_{ts} are the vibrational partition functions of the initial equilibrium state and the transition state, respectively. The Z function is correlated to the Helmholtz free energy F [39]:

$$F = -k_B T lnZ = k_B T \sum_{\mathbf{q}_i}^{N} ln\left[2sinh\left(-\frac{hw_{\mathbf{q}_i}}{2k_B T}\right)\right] \tag{3}$$

where $w_{\mathbf{q}_i}$ is the i mode frequency in the $\mathbf{q}$ point and the sum is over all the modes.

In order to obtain the diffusion coefficient of a species in a crystal lattice, all the possible jumping paths need to be identified and their relative jumping rates need to be found through Eq. 1-2-3 .

Diffusion in crystal lattices can be quite complex, since an atom can randomly jumps between several crystallographic sites. In these cases, the Monte Carlo approach can be used to find diffusion coefficients. In alternative, an analytical Multi-State Diffusion method has been proposed by Landman [29, 30] for finding the diffusion coefficients of an atomic species in a crystal lattice [31, 34, 32]. This method is detailed elsewhere [29, 30], only the main steps are summarized herein. First, one needs to identify all the N different kinds of jumps, each of which is identified by a displacement and a waiting time distribution function. The NxN Laplace transform matrix of the waiting-time function, $\underline{\psi}(u)$, and the NxN Fourier transform matrix of the displacements, $\underline{p}(\overrightarrow{k})$, are stated. The propagator matrix $\underline{R}(\overrightarrow{k}, u)$ is hence calculated as following:

$$\underline{R}(\overrightarrow{k}, u) = [\underline{I} - \underline{p}(\overrightarrow{k}) \odot \underline{\psi}(u)]. \tag{4}$$

The diffusive variance $\sigma_r^2(t)$ along any r direction is:

$$\sigma_r^2(t) = \lim_{\vec{k}\to 0} t\frac{1}{\Delta_0}\frac{\partial^2\Delta}{\partial k_r^2}\Big|_{u\to 0} \tag{5}$$

with Δ indicating the determinant of $\underline{R}$ and Δ_0 is

$$\Delta_0 = \lim_{u\to 0}\frac{\Delta(\vec{k},u)}{u} \tag{6}$$

At last, the diffusion coefficient along r is :

$$D_r = \frac{\sigma_r^2(t)}{2t}. \tag{7}$$

2.2. DFT Computations

Electronic structure calculations were carried out with the VASP *Ab initio* code [37, 38], solving the self-consistent Kohn-Sham equations with the projector augmented wave (PAW) pseudopotentials [40]. The Perdew-Burke-Ernzerhof (GGA-PBE) exchange and correlation functionals have been adopted in this study [41]. Convergence tests have been performed to determine the plane-wave energy cutoff and the k-point number, in order to obtain a numerical accuracy of 10^{-6} eV. The cutoff was hence set at 550 eV and the k-points number equal to 1000 for the conventional unit cell of γ-TiAl, containing 4 atoms. The density of k-points was kept approximately constant for the supercell calculations. The study of the interstitial carbon and nitrogen defects was performed on 3 x 3 x 3 super-cells, containing 109 atoms. The size was chosen after performing some convergence tests on 2 x 2 x 2, 3 x 3 x 3 and 4 x 4 x 4 super-cells in order to evaluate the finite-size effect. The energy difference between the 3x3x3 and 4 x 4 x 4 cells was inferior to 0.03 eV/atom, which is an acceptable small value. For the structural optimization, the lattice cell parameters and all the atomic positions were relaxed.

The NEB calculations were also performed on 3 x 3 x 3 super-cells, with a number of images comprised between 5 and 7, depending on the specific path. For the NEB calculations, all the atomic positions were let to vary, while the cell parameters were fixed. This choice was made because letting vary the cell parameters would lead to super-cells of different dimensions among the images of the NEB calculation and this often leads to convergence problems. As the relaxations of the various interstitial defects lead to slightly different cell parameters (difference $\leq$ 0.01 Å), a choice had to be made. Therefore, all the NEB calculations were performed using the cell parameters obtained for the most stable interstitial defect (the other interstitial positions used as starting/end point for the NEB were hence relaxed in this fixed cell configuration before starting the NEB). A convergence of 10^{-4} eV on the image with maximum energy was systematically reached for the NEB calculations The finite displacement method (FDM), as implemented in the *phonopy* code [42], was used for the vibrational properties. These calculations were also performed on 3 x 3 x 3 super-cells, with the same numerical parameters (energy cutoff, k-points density and energy convergence criteria) used for the relaxations. In addition, a convergence criterion of 10^{-7} eV/Å was also set on the forces.

2.3. Crystal structure and interstitial sites

The $L1_0$-TiAl phase crystallizes in the tetragonal $P4/mmm$ space group (N° 123), with Al and Ti atoms in the *1a* and *1d* Wyckoff positions, respectively. The primitive unit cell, shown in Fig.1-(b), contains two atoms. The computed lattice parameters, equal to a = 2.829 Å and c = 4.073 Å, are in good agreement with the experimental data (a = 2.828 Å and c = 4.075 Å [43]).

Equivalently, the $L1_0$-TiAl structure is generally represented with a pseudo-cubic conventional unit cell, with a c/a ratio close to unity. In this case, the pattern consists of 3 atoms, for instance two Al atoms at $(0, 0, 0)_C$ and $(1/2, 1/2, 1/2)_C$ and one Ti at $(0, 1/2, 1/2)_C$, as shown in Fig.1-(a). The c indices here highlight that the coordinates are expressed in the pseudo-cubic cell. This conventional cell is rotated of 45° around the z axis with respect to the primitive one. This description is advantageous since it reveals the underlying fcc network. Indeed, the $L1_0$ is an ordered structure of the fcc lattice, with a modulation of composition along the c axis.

As commonly known, the *fcc* lattice (similarly to the *hc* lattice) can be described as a regular packing of octahedra and tetrahedra. In *fcc* metals, the atoms are located at the vertices of the polyhedra, leaving in their centres cavities that

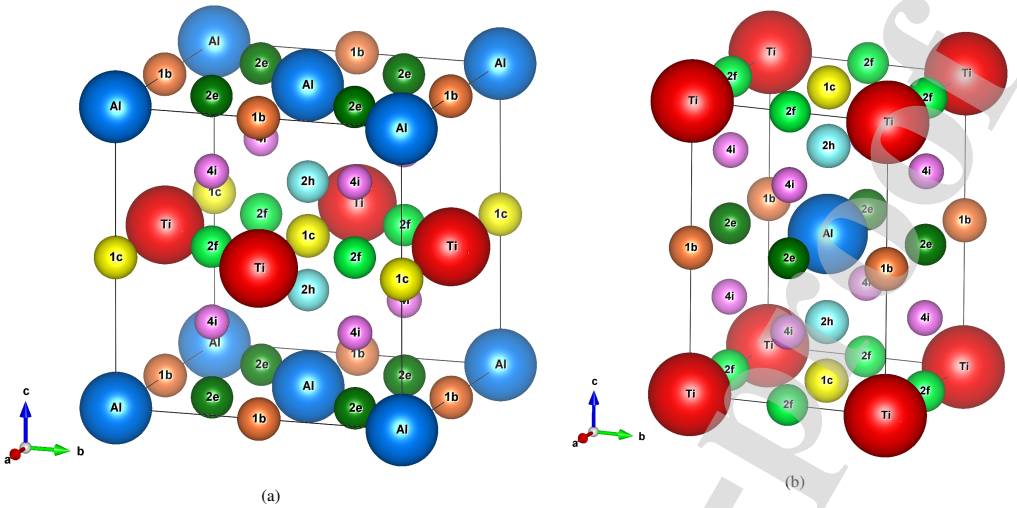

Figure 1: Two equivalent representations of the γ-TiAl crystal structure: (a) distorted face-centred and (b) body-centred tetragonal. The various interstitial positions tested are also shown.

can generally easily host interstitial atoms. In the $L1_0$-TiAl structure, due to the ordering of Al and Ti, there are two regular octahedral sites, corresponding to the Wyckoff positions *1c* and *1b*, and one tetrahedral site, corresponding to the *4i* position, see Fig. 1. The latter is the centre of a tetrahedron with, at the corners, two Al and two Ti atoms, and it will be more intuitively noted as Ti_2Al_2. The tetrahedral site is smaller than the octahedral ones. It has been shown that this position plays and important role in the diffusion of hydrogen in γ-TiAl [36], while the accommodation of larger atoms such as boron [26] and oxygen [26, 27] is less favoured and hence less important for the diffusion. The *1c* position coincides with the centre of an octahedron formed by four Ti and two Al atoms, and it will also be indicated as Ti_4Al_2. The *1b* position is the center of an octahedron formed by four Al and two Ti atoms, hence named Al_4Ti_2. In previous studies [25], these two octahedra have supposed to be the most stable positions for interstitial atoms, such as B, C, N and O. However, the high symmetry of these positions can lead to false results in DFT calculations and the dynamical stability of such defects needs to be verified. For instance, Epifano and Hug [26] have recently shown that these octahedral sites are indeed the most stable positions for boron, but not for oxygen. An oxygen atom in the *Ti4Al2* site has a vibrational instability along the z direction, which makes it to shift toward the *2h* Wyckoff position [26]. This is the stable site for the oxygen species in γ-TiAl. A metastable site for oxygen, according to [26], is the *2e* Wyckoff position, which is on the edge of the *Al4Ti2* octahedron, between two Al atoms. This position corresponds to the centre of a non-regular octahedron, with two equidistant Al atoms, at ~1.80 Å, and four farther Ti atoms, at ~2.3 Å [26]. Connetable *et al.* obtained similar results [27], confirming that oxygen is not stable in the centre of the regular octahedra and that stable sites are *2h* and *2e*. These authors tested also additional interstitial sites and found other stable positions for oxygen: the *Ti2Al2* (*4i*) site, and other similar tetrahedral positions (*4k* and *4m*). However, these sites are characterized by quite high insertion energies and consequent low escape energy barriers: this means that the probability to reach these sites and the associated residence times are small. Indeed, Connetable *et al.* showed that these sites can be neglected for the diffusion coefficient calculations [27].

In summary, based on the lattice symmetry and the previous studies, the *1c*, *1b*, *4i*, *2h*, *2e* Wyckoff positions were tested for carbon and nitrogen. In addition, the *2f* position has also been tested: this site is specular to the *2e* position, but it lies on the Ti basal plane. All the investigated sites are shown in Fig. 1.

3. Results

3.1. Relaxation of C and N interstitial atoms

Six interstitial positions have been tested for the C and N insertion in γ-TiAl, as explained in 2.3. These sites are summarized in table 1 and shown in Fig. 1. One interstitial atom has been added in a 3x3x3 cell containing 108 atoms (54 Al and 54 Ti). In order to find the minimum energy configuration, the unit cell parameters and all the atomic positions have been let to vary. The relative enthalpy of formation is calculated as:

$$H_f = \frac{1}{N}\left(E_{tot} - \sum_i^N \mu_i\right) \tag{8}$$

where E_{tot} is the total energy obtained by DFT for a cell of N atoms and μ_i is the chemical potential of the atomic species i, in its reference state (provided in Appendix A). Herein, we used the usual approximation to substitute it with the energy calculated at 0 K for the atomic species i. The insertion energy for the interstitial atom I is expressed by:

$$E_i = E_{tot}[TiAl + I] - E_{tot}[TiAl] - E_I^{ref} \tag{9}$$

where E_I^{ref} is the reference state of the interstitial (graphite for carbon and $\frac{1}{2}N_2$ molecule for nitrogen). The results for C and N insertion in the various interstitial positions are summarized in Table 1.

		1c (Ti_4Al_2)	*1b* (Al_4Ti_2)	*4i* (Ti_2Al_2)	*2h*	*2e*	*2f*
		stable	**stable**	unstable	unstable	**stable**	unstable
	E_i	-0.516	0.995	4.348	3.225	1.604	2.961
TiAl+C	H_f	-0.409	-0.395	-0.364	-0.374	-0.389	-0.377
	ΔH_i	0	0.014	0.045	0.035	0.020	0.032
		stable	**stable**	unstable	unstable	**stable**	unstable
	E_i	-2.065	-0.606	1.364	0.660	-0.569	-
TiAl+N	H_f	-0.423	-0.409	-0.391	-0.398	-0.409	-
	ΔH_i	0	0.013	0.032	0.025	0.014	-

Table 1: Insertion energies E_i (eV), enthalpy of formation H_f (eV/atom) of carbon and nitrogen in various positions of γ-TiAl. ΔH_i represents the difference in energy (eV/atom) between the most stable site, which is *1c* for both the C and N, and the other positions.

The DFT calculations clearly showed that some of the investigated configurations are unstable: *4i*, *2h* for carbon; *4i*, *2h* and *2f* for nitrogen. For all these sites, the energies reported in Table 1 are quite high. For these positions, the complete relaxation (cell parameters and all the atomic positions) resulted in a displacement of the C and N atoms toward other interstitial sites. For instance, the *2h* Wyckoff position (1/2, 1/2, ±z) has been evaluated by applying a shift of $\Delta z = 0.02$Å from the centre of the Ti_4Al_2 octahedron. During the relaxation, both C and N returned to the centre, corresponding to the *1c* site. Similarly, when inserted in the *4i* site, N and C moved toward the *2e* position. Also during the relaxation of the *2f* position, N moved toward *2e*, while carbon remained in that site. For these unstable sites, the energy values reported in Table 1 were obtained by fixing the atomic positions of the defect during the calculations (while the cell parameters and the other atomic positions were let to vary)

Therefore, after DFT relaxation, four interstitial positions seem possible for carbon accommodation (*1c, 1b, 2e* and *2f*) and three for nitrogen (*1c, 1b, 2e*). However, the static relaxation is not sufficient to conclude on the stability of the interstitial positions. Indeed, in some of these configurations, forces can vanish for symmetry reasons only and hence their dynamical stability needs to be verified. For this reason, inter-atomic force constants have been analysed. The results are displayed, as phonon density of states, in Fig. 2 and Fig. 3, for carbon and nitrogen, respectively.

Considering the carbon insertion, the configurations with the interstitial in *1c*, *1b* and *2e* show only positive vibrational frequencies, confirming their stability or metastability. On the contrary, when carbon is inserted in the *2f* position, an imaginary frequency appears around -11 THz, indicating that this configuration is not a local minimum.

For nitrogen, all the three remaining configurations *1c*, *1b* and *2e* show only positive frequencies, confirming that they are stable or metastable.

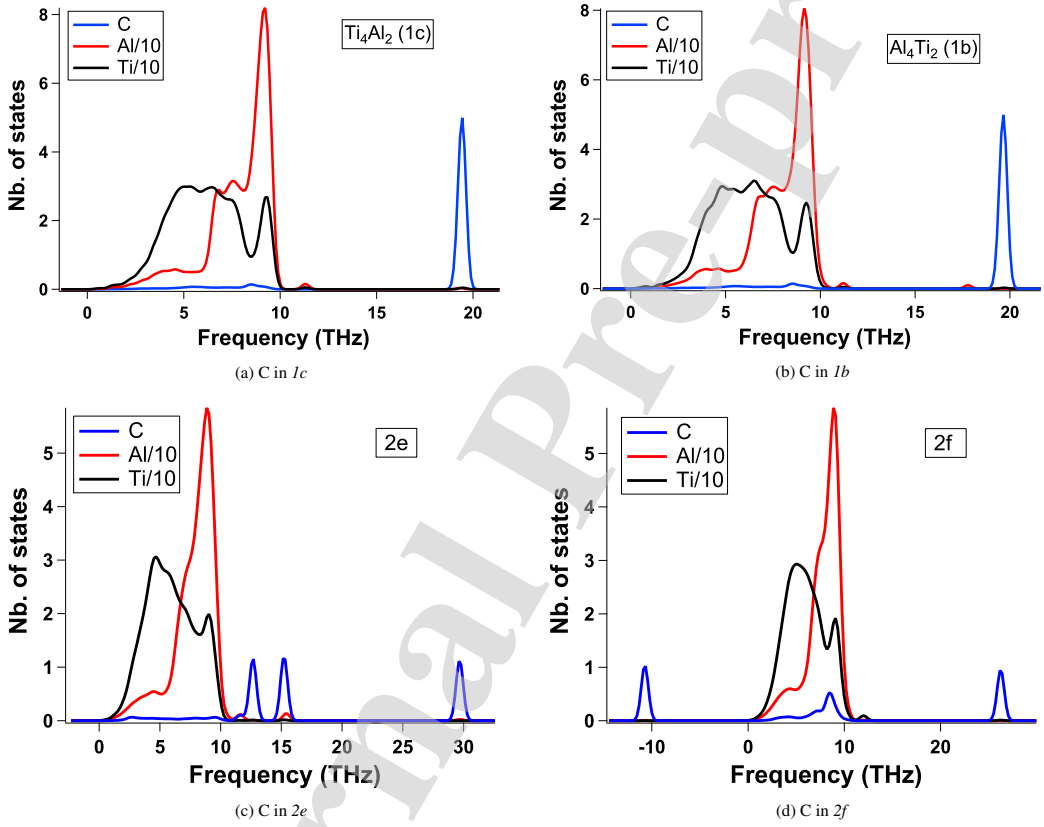

(a) C in *1c*

(b) C in *1b*

(c) C in *2e*

(d) C in *2f*

Figure 2: Projected density-of-states (pDOS) of C in *1c*, *1b* and *2e* sites (from top to the bottom). The amplitudes of the pDOS onto Ti and Al were divided by 10.

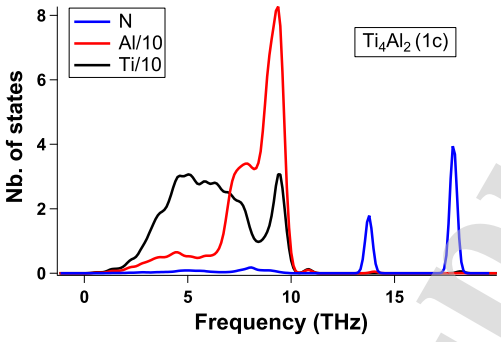

(a) N in *1c*

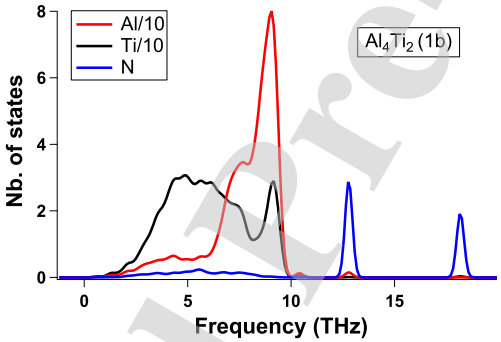

(b) N in *1b*

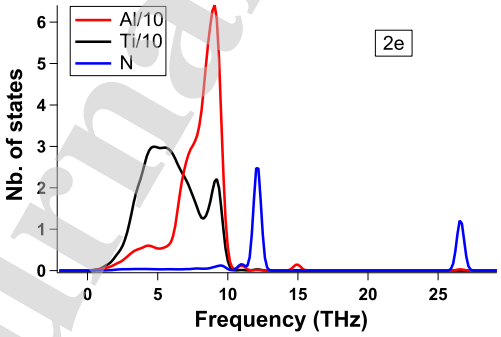

(c) C in *2e*

Figure 3: Projected density-of-states (pDOS) of N in *1c*, *1b* and *2e* sites (from top to the bottom). The amplitudes of the pDOS onto Ti and Al were divided by 10.

In summary, for both C and N, three possible interstitial sites have been identified: *1c*, *1b* and *2e*. For both the elements, the most stable position is *1c* (Ti_4Al_2), i.e., the octahedral site richer in titanium. The associated insertion energy is negative for both C and N, indicating that the accommodation of these species is favoured. In particular, the value obtained for nitrogen is < -2 eV, indicating a high affinity for this Ti-rich site. These results are consistent with those previously obtained for other species, such as boron and oxygen [26]. For the former, the stable position is also the *1c* site. For oxygen, as already discussed in section 2.3, the centre of the Ti_4Al_2 octahedron presents an instability along *z*, and the stable position is *2h*, but it still coincides with the environment richer in titanium.

Other metastable interstitial positions are present on the (001) Al basal plane, but in this case the situation is more complex and it differs from species to species. In order to visualize the differences, energy maps of this plane have been calculated for C, N and O. The color plot has been obtained as following: the interstitial atom was placed in each position of the plane, by fixing its *x* and *y* coordinate; then, DFT calculations were performed, relaxing all the other atomic coordinates, except the *x*, *y* of the interstitial atom (but including its *z* coordinate). The results are shown in Figure 4.

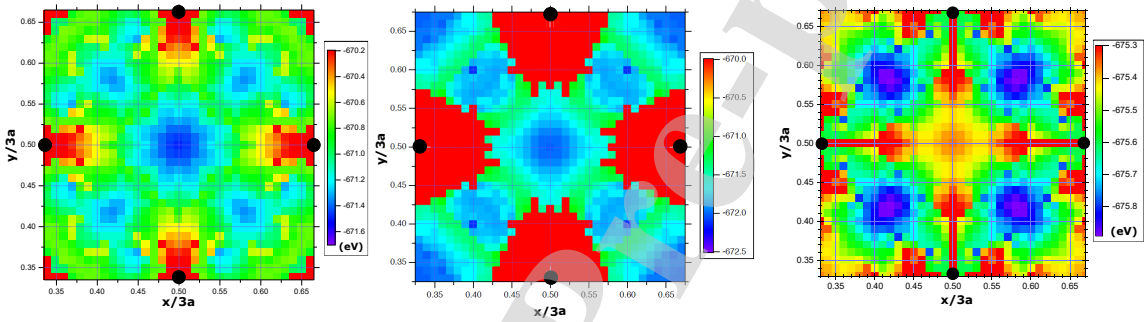

(a) Carbon (b) Nitrogen (c) Oxygen

Figure 4: Energy chart of the (001) plane constituted of Al atoms with C, N and O interstitial atoms. Each point on the charge represents the resulting energy when the interstitial atom is placed in that position.

As already proved, C can be accommodated in two positions of the Al basal plane: *1b* and *2e*, which coincide with the centre and the edge of the Al_4Ti_2 octahedron, respectively. This is clearly shown by the map of Fig. 4-(a), where these sites correspond to the blue areas (lowest energies). For carbon, the centre of the octahedron is more stable than the *2e* site. However, it must be noticed that, for both the positions, the insertion energies have positive values, contrary to that of the *1c* site. Similarly to carbon, also nitrogen can be accommodated in both *1b* and *2e* positions. However, in this case, the two configurations have almost identical energies. Moreover, contrary to carbon, the insertion energies for these two sites have negative values. Finally, a remarkable difference is observed in the oxygen map (Fig. 4-c), where a local maximum is observed in the centre of the octahedron. Indeed, oxygen is not stable in this site and it can only be accommodated in the edges (the *2e* position). In [26], the opposite situation was reported for boron: this interstitial is accommodated in the centre of the octahedron but not in the edges. Therefore, comparing B, C, N and O, a regular evolution is observed in the Al basal plane: the stable position moves from the *1b* toward the *2e* site by increasing the *Z* number of the interstitial.

3.2. *Diffusion paths and energy barriers*

In order to determine the diffusion coefficient of an interstitial atom in a crystal lattice, one needs to determine the energy barrier associated to the atomic jump between two interstitial sites. Each jump represents a single step in the diffusion process of the solute atom. As shown in 3.1, both carbon and nitrogen can be found in various interstitial sites in γ-TiAl and hence several diffusive paths are possible. For each of them, the minimum energy path and the relative energy barrier were found using the CI-NEB method.

Specifically, for N and C, three stable interstitial sites have been identified in γ-TiAl: *1c*, *1b* and *2e*. Combining these, six jumps toward first neighbour sites are possible in total, which are shown in Fig. 5 and summarized in table 2.

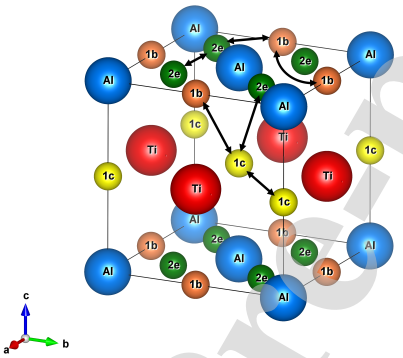

Figure 5: Interstitial sites where N and C can be accommodated in γ-TiAl and paths for diffusion.

On the γ-TiAl(001) plane constituted of Al atoms, the *1b* and *2e* sites are present. Three jumps are possible among them on this plane: $1b \leftrightarrows 1b$, $2e \leftrightarrows 2e$ and $1b \leftrightarrows 2e$. Of these three, only the latter corresponds to a single step process: for both C and N, all the NEB calculations between two equal sites lead to a path crossing the other position. Therefore, only the $2e \leftrightarrows 1b$ path is retained for the diffusion. In addition, when the diffusing atom is in *2e* or *1b*, it can also jump toward the *1c* site, with a displacement also along the z direction. The NEB computations showed that both the $1b \leftrightarrows 1c$ and $2e \leftrightarrows 1c$ paths are possible for N. On the contrary, for C, the NEB calculations showed that the $1c \leftrightarrows 2e$ path is not energetically favoured: the interstitial atom is driven toward the *1b* site. Finally, the last possible path is between two neighbouring *1c* sites, which are on the γ-TiAl(001) plane constituted of Ti atoms.

In summary, after the NEB computations, three single-step paths are obtained for carbon and four for nitrogen. For each of this and for each direction, the obtained energy barriers are reported in Table 2.

The diffusion energy barriers of carbon and nitrogen present several similarities. For both the species, the highest barrier values are associated to the jumps from the *1c* (Ti_4Al_2) position. In particular, the highest energy barrier is associated to the $1c \leftrightarrows 1c$ path, with values above 3 eV (3.342 eV and 3.539 eV, for N and C, respectively). The energy barrier associated to the $1c \rightarrow 1b$ jump is lower, but still quite high, with values equal to 2.163 and 2.542 eV, for N and C, respectively. For nitrogen, the additional possible path from *1c* toward *2e* has a energy barrier similar to the previous one (2.206 eV), as expected since the configurations with N in the *1b* and *2e* sites have very close energy.

The high energy barriers obtained for the *1c* site confirm that the centre of the Ti-rich octahedron is a very stable position for both C and N, hence it acts as a trap for their diffusion. The diffusion along the z direction is expected to be low, since this occurs necessarily through jumps crossing alternatively the Ti and Al basal plane. On the contrary, the diffusion in the xy direction can proceeds faster in the Al basal planes, through jumps among the *1b* and *2e* positions, whose energy barriers are lower than 1 eV, for both C and N. Therefore, the diffusion of C an N in γ-TiAl is expected to be anisotropic.

According to transitional state theory of Eyring, previously presented in section 2, the pre-factor of the jumping rate associated to each diffusion path can be obtained from the phonon modes of the starting and transitional states. For

Path			Energy barrier (eV)	
Start	End	Distance (Å)	N	C
1c	*1c*	≃ 2.8	3.342	3.539
1b	*1b*	≃ 2.8	=1b→2e→1b	
2e	*2e*	≃ 2.0	=2e→1b→2e	
1c	*1b*	≃ 2.8	2.163	2.542
1b	*1c*	≃ 2.8	0.758	1.031
1c	*2e*	≃ 2.5	2.211	=1c→1b→2e
2e	*1c*	≃ 2.5	0.980	=2e→1b→1c
2e	*1b*	≃ 1.4	0.475	0.379
1b	*2e*	≃ 1.4	0.633	0.989

Table 2: Migration energies for N and C in γ-TiAl.

this reason, phonon calculations were performed for the maximum energy configurations obtained from the previous NEB computations. The results are presented, as phonon density of states, in Fig. 6 and Fig. 7, for N and C, respectively.

For nitrogen diffusion, one single imaginary vibrational mode is observed for the transitional states of the 1c⇆1b and 1b⇆2e paths. These configurations correspond hence to saddle points. On the contrary, in each of the other two paths, two imaginary vibrational modes are observed, indicating that these configurations correspond to transitional states of second order. Considering the $1c \leftrightarrows 1c$ jump, the transitional state as well as all the images of the previous NEB optimization lie on the (001) plane formed by Ti. The NEB computations for this path were repeated by imposing to the middle image an initial displacement of $\Delta z = 0.01$Å from the (001) plane. The new optimized path obtained in this way lies between the Ti and Al basal planes and it passes through the *1b* site. This indicates that, in the previous calculation, the forces along z were cancelled by symmetry. It can be concluded that the lowest energy path for nitrogen escaping from the *1c* site coincides to the $1c \rightarrow 1b$. The other two jumps are not favoureble, since second order transition states are associated to these paths. Indeed, as Connetable *et al.* showed for the diffusion of H and O in various *fcc* metals [39], these states provide a minor contribution to the diffusion.

For carbon, one single imaginary mode was found for the maxima-energy points of the three considered paths (1b-2e,1c-1c, 1c-1b), which can hence be identified as saddle points.

3.3. Diffusion coefficients

The temperature-dependent jumping rates of nitrogen and carbon in γ-TiAl were obtained using Eq. 1-3. The diffusion coefficients along the *xy* and *z* crystallographic directions were then obtained using the Multi-State Diffusion method explained in section 2.1. Details on the matrix expressions for each case are provided in Appendix B. For nitrogen, only the first-order transition states identified in the previous section, corresponding to the $1c \leftrightarrows 1b$ and $1b \leftrightarrows 2e$ diffusion paths, were considered. The inclusion of the second order transition states lead to a negligible difference, as it is shown in the Appendix C.

The computed diffusion coefficients of C and N are compared to the oxygen case [26] in Fig. 8, for $1050 \lesssim T \lesssim 1550$ K. In this temperature range, the highest values are exhibited by oxygen, even if the diffusion coefficients of carbon intersect and exceed those of oxygen for $T > 1400$ K. Nitrogen presents the lowest diffusion coefficients.

One can also remark that oxygen and nitrogen exhibit a marked anisotropic diffusion, with $D_{xy} > D_z$. On the contrary, the anisotropy is much less important for carbon. A low anisotropy was also previously reported for boron diffusion in γ-TiAl [26]. As discussed in section 3.1, a regular relative decrease in the insertion energy is observed between the *1c* and *2e* sites of the the Al basal plane, from boron to oxygen. The *1c* has a lowest energy configuration for boron and carbon, while *2e* is preferable for nitrogen and oxygen. This difference is likely the origin of the higher anisotropy obtained for the N and O diffusion coefficients: the *2e* sites enhance the diffusion in the *xy* directions.

From the computed diffusion coefficients, we obtained the Arrhenius equations:

$$D(T) = D_0 \cdot e^{-\Delta E / k_b T} \tag{10}$$

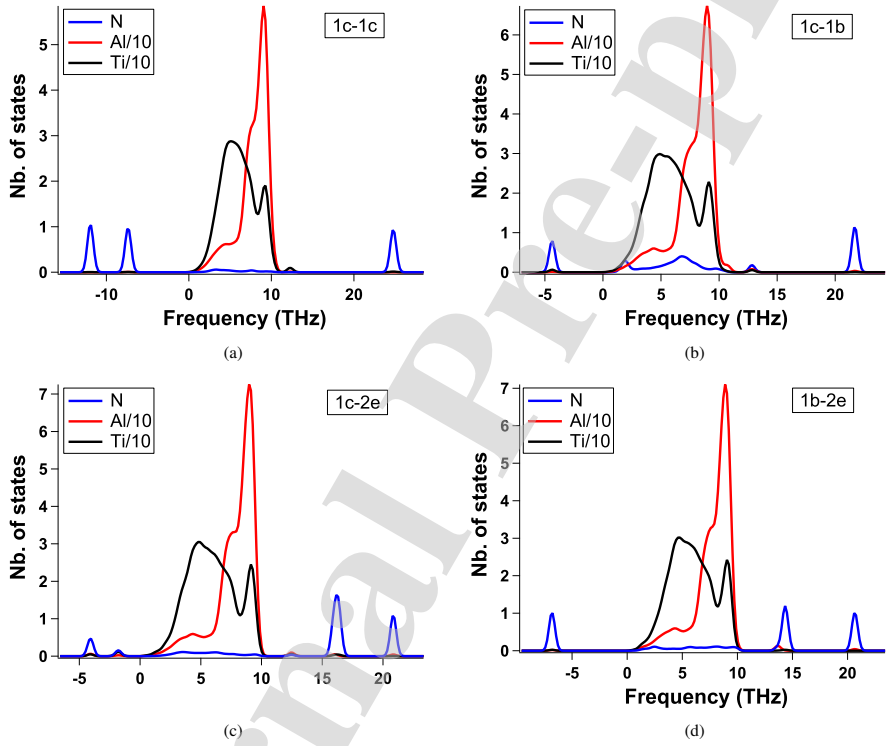

Figure 6: PDOS of N in the maximum energy point associated to the different diffusion path:(a) 1c⇆1c, (b) 1c⇆1b, (c) 1c⇆2e, (d) 1b⇆2e.

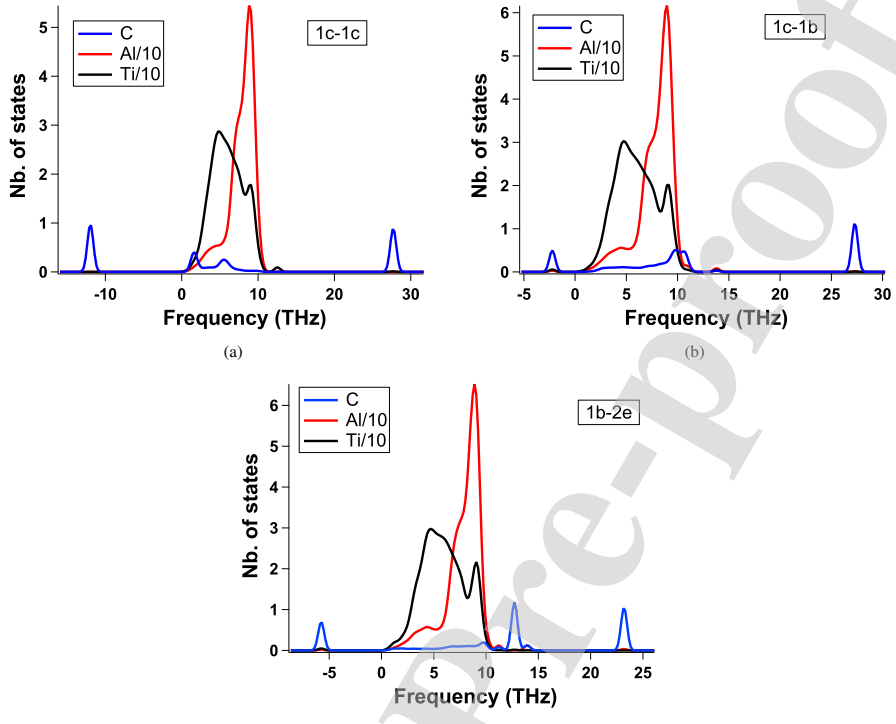

Figure 7: PDOS of C in the maximum energy point associated to the different diffusion path:(a) 1c⇆1c, (b) 1c⇆1b, (c) 1b⇆2e.

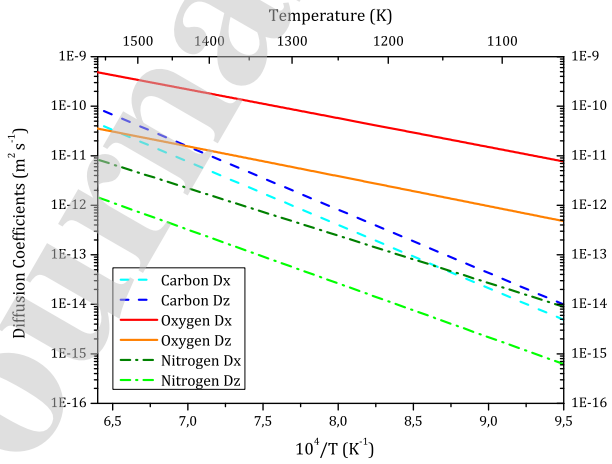

Figure 8: Computed diffusion coefficients of carbon and nitrogen (this work), compared to those of oxygen [26] in γ-TiAl.

with D_O and Δ_E values reported in Table 3.

Species	D_0(xy) (m^2s^{-1})	ΔE(xy) (eV)	D_0(z) (m^2s^{-1})	ΔE(z) (eV)
C	$6.05 \cdot 10^{-3}$	2.53	$1.22 \cdot 10^{-2}$	2.52
N	$1.20 \cdot 10^{-5}$	1.91	$1.22 \cdot 10^{-5}$	2.15
O [26]	$3.5 \cdot 10^{-6}$	1.18	$3.4 \cdot 10^{-7}$	1.21

Table 3: Computed activation energies and pre-factors for the diffusion coefficients of carbon, nitrogen and oxygen [26].

Oxygen exhibits the lowest activation energies for diffusion, followed by nitrogen and carbon. This is also shown by the different slopes in Fig. 8. Higher activation energies imply that higher temperatures are necessary to activate diffusion. As discussed in section 1, N diffusion in γ-TiAl is of particular interest because nitrides (TiN and Ti_2AlN) are formed (in addition to Al_2O_3 and TiO_2) during the oxidation of titanium aluminides under air [5, 4, 7, 8]. Becker *et al*. investigated the oxidation in air of Ti-Al alloys, for temperatures ranging from 973 K to 1273 K [5]. This work showed that the formation of nitrides is temperature dependent: TiN and Ti_2AlN started to be observed for T > 1073 K, with content increasing with temperature. The relatively high activation energy for nitrogen diffusion in γ-TiAl could be one of the reason why the nitrides are not observed for low temperature oxidations.

4. Conclusions

The insertion and diffusion of C and N in γ-TiAl have been investigated using a DFT-based method. Several interstitial positions (*1c, 1b, 4i, 2h, 2e, 2f*) of the $L1_0$-TiAl structure were evaluated, combining DFT structural relaxation and phonon calculations. For both C and N, the most stable interstitial position is found to be the *1c* site, which corresponds to a regular octahedron formed by 4 Ti and 2 Al atoms. In addition, two metastable sites have been identified on the (001) plane formed of Al atoms, namely *1b* and *2e*. The first corresponds to a regular octahedron formed of 4 Al and 2 Ti atoms; the latter is a distorted octahedron, formed of 2 close Al atoms and 4 farther Ti atoms. Carbon exhibits a lowest insertion energy for the *1b* site rather than the *2e*, while the two positions are almost identical for nitrogen. Comparing these results with those previously reported for boron and oxygen [26], a regular variation can be observed: on the Al-(001) plane, by increasing the Z number of the interstitial atom, the favourable configuration moves from the *1b* site (the only possible for B) to the *2e* site (the only possible for O).

The possible jump paths of C and N among the *1c*, *1b* and *2e* were then investigated by NEB. From these, the diffusion coefficients of C and N along the different crystallographic directions were obtained and compared to those previously reported for oxygen [26]. For all the species, the computations indicated an anisotropic diffusion behaviour. This is particularly true for oxygen and nitrogen, which exhibits a diffusion coefficient along the *xy* directions much higher than the *z* direction, while the anisotropy is very limited for carbon. This difference is likely due to an enhanced diffusion in the Al-(001) plane through the *2e* sites, in which N and O are more easily inserted.

Comparing the diffusion coefficients of C, N and O in the 1050-1550 K temperature range, oxygen exhibits the highest values, followed by carbon and nitrogen. The diffusion activation energies of nitrogen (1.91 eV for *xy* , 2.15 eV for *z*) and carbon (2.53 eV for *xy* , 2.52 eV for *z*) are higher than those of oxygen (1.18 eV for *xy* , 1.21 eV for *z*), which implies that the C and N diffusion coefficients increase more rapidly with temperature than those of oxygen. For instance, at T $\simeq$ 1050 K, the O diffusion coefficients are $10^2 - 10^3$ times higher than those of C and N, while at T $\simeq$ 1500 K they are comparable with those of carbon and only 1-2 orders of magnitude higher than those of nitrogen.

The diffusion coefficients data here obtained represent fundamental quantities to understand and predict diffusion-controlled reactions, as for instance oxidation of Ti-Al alloys. Indeed, these data can be used as input for kinetic databases which allow predicting the evolution of materials during oxidation.

Appendix A. Energies of pure elements in their reference state

Table A.4: Reference total energies (E_{tot}) of the elements.

Element	structure	E_{tot} (eV.atom^{-1})
Ti	*hc*	-7.890
Al	*fcc*	-3.747
C	graphite	-9.216
N_2	molecule	-8.309

Appendix B. Multi-state diffusion model

The diffusion coefficients were computed using the the analytical, multi-state diffusion method proposed by Landaman [29, 30]. Herein, we report the Laplace transform of the waiting time density matrix, $\underline{\psi}(u)$, and the Fourier transform of the displacement matrix, $\underline{p}(\overrightarrow{k})$, for the diffusion of C and N in γ-TiAl.

First, we need to define a unit cell and identify the number of interstitial sites present in it. We selected as unit cell the one shown in Fig. 5, where Al and Ti atoms are represented in blue and red, respectively, and the interstitial sites are in yellow (*1c*), green (*2e*) and orange (*1b*). In this conventional cell, there are two *1c* positions, two *1b* sites and four *2e*. In the most general case encountered in this work, four single-step paths are possible: $1b \rightleftarrows 1c$, $1b \rightleftarrows 2e$, $1c \rightleftarrows 1c$, $1c \rightleftarrows 2e$. On the contrary, direct jumps between two *1b* and two *2e* sites are not possible.

The Laplace transform of the waiting time density matrix $\underline{\psi}(u)$ is given by:

$$\underline{\psi}(u) =$$

$$\begin{array}{c} \\ 1b \\ 1b \\ 1c \\ 1c \\ 2e \\ 2e \\ 2e \\ 2e \end{array}
\begin{array}{c}
\begin{array}{cccccccc} 1b & 1b & 1c & 1c & 2e & 2e & 2e & 2e \end{array} \\
\begin{pmatrix}
0 & 0 & \frac{4\nu_{1c1b}}{K_{1c}(u)} & \frac{4\nu_{1c1b}}{K_{1c}(u)} & \frac{\nu_{2e1b}}{K_{2e}} & \frac{\nu_{2e1b}}{K_{2e}} & \frac{\nu_{2e1b}}{K_{2e}} & \frac{\nu_{2e1b}}{K_{2e}} \\
0 & 0 & \frac{4\nu_{1c1b}}{K_{1c}(u)} & \frac{4\nu_{1c1b}}{K_{1c}(u)} & \frac{\nu_{2e1b}}{K_{2e}} & \frac{\nu_{2e1b}}{K_{2e}} & \frac{\nu_{2e1b}}{K_{2e}} & \frac{\nu_{2e1b}}{K_{2e}} \\
\frac{4\nu_{1b1c}}{K_{1b}(u)} & \frac{4\nu_{1b1c}}{K_{1b}(u)} & 0 & \frac{4\nu_{1c1c}}{K_{1c}(u)} & \frac{2\nu_{2e1c}}{K_{2e}(u)} & \frac{2\nu_{2e1c}}{K_{2e}(u)} & \frac{2\nu_{2e1c}}{K_{2e}(u)} & \frac{2\nu_{2e1c}}{K_{2e}(u)} \\
\frac{4\nu_{1b1c}}{K_{1b}(u)} & \frac{4\nu_{1b1c}}{K_{1b}(u)} & \frac{4\nu_{1c1c}}{K_{1c}(u)} & 0 & \frac{2\nu_{2e1c}}{K_{2e}(u)} & \frac{2\nu_{2e1c}}{K_{2e}(u)} & \frac{2\nu_{2e1c}}{K_{2e}(u)} & \frac{2\nu_{2e1c}}{K_{2e}(u)} \\
\frac{\nu_{1b2e}}{K_{1b}(u)} & \frac{\nu_{1b2e}}{K_{1b}(u)} & \frac{2\nu_{1c2e}}{K_{1c}(u)} & \frac{2\nu_{1c2e}}{K_{1c}(u)} & 0 & 0 & 0 & 0 \\
\frac{\nu_{1b2e}}{K_{1b}(u)} & \frac{\nu_{1b2e}}{K_{1b}(u)} & \frac{2\nu_{1c2e}}{K_{1c}(u)} & \frac{2\nu_{1c2e}}{K_{1c}(u)} & 0 & 0 & 0 & 0 \\
\frac{\nu_{1b2e}}{K_{1b}(u)} & \frac{\nu_{1b2e}}{K_{1b}(u)} & \frac{2\nu_{1c2e}}{K_{1c}(u)} & \frac{2\nu_{1c2e}}{K_{1c}(u)} & 0 & 0 & 0 & 0 \\
\frac{\nu_{1b2e}}{K_{1b}(u)} & \frac{\nu_{1b2e}}{K_{1b}(u)} & \frac{2\nu_{1c2e}}{K_{1c}(u)} & \frac{2\nu_{1c2e}}{K_{1c}(u)} & 0 & 0 & 0 & 0
\end{pmatrix}
\end{array} \tag{B.1}$$

where ν_{jk} is the jumping rate from site j to site k and

$$K_{1b}(u) = 4\nu_{1b2e} + 8\nu_{1b1c} + u; \tag{B.2}$$

$$K_{1c}(u) = 4\nu_{1c1c} + 8\nu_{1c1b} + 8\nu_{1c2e} + u. \tag{B.3}$$

$$K_{2e}(u) = 2\nu_{2e1b} + 4\nu_{2e1c} + u. \tag{B.4}$$

The vector $\overrightarrow{l_k} - \overrightarrow{l_j} = m_1\overrightarrow{l_1} + m_2\overrightarrow{l_2} + m_3\overrightarrow{l_3}$ is the displacement of an atom jumping from the site j to the site k. The element $p_{jk}(\overrightarrow{k})$ of the $\underline{p}(\overrightarrow{k})$ matrix is

$$p_{jk}(\overrightarrow{k}) = \frac{\sum_{h=1}^{N_{jk}} \delta_{jk}^{h}}{N_{jk}} \tag{B.5}$$

where the sum is over all the considered paths from a site j to a site k and

$$\delta_{jk}^{h} = e^{i(m_k^1 l_1 \overrightarrow{k_1} + m_k^2 l_2 \overrightarrow{k_2} + m_k^3 l_3 \overrightarrow{k_3})} \tag{B.6}$$

where m_k can be equal to 0 or ± 1. It is equal to 0, if the site k is in the same cell, or to ± 1, if the k site is in another cell and the sign indicates the direction in which the cell is repeated.

The Fourier transform matrix of the displacement is then:

$\underline{p}(\overrightarrow{k}) =$

$$\begin{array}{c} \\ 1b \\ 1b \\ 1c \\ 1c \\ 2e \\ 2e \\ 2e \\ 2e \end{array} \begin{array}{c} \begin{array}{cccccccc} 1b & 1b & 1c & 1c & 2e & 2e & 2e & 2e \end{array} \\ \begin{pmatrix} 0 & 0 & H & Q & 1 & 1 & Y & G \\ 0 & 0 & I & R & 1 & Y & 1 & D \\ A & E & 0 & S & Pp & X & W & Z \\ B & F & L & 0 & Z & U & T & Aa \\ 1 & 1 & M & P & 0 & 0 & 0 & 0 \\ 1 & C & N & T & 0 & 0 & 0 & 0 \\ C & 1 & O & U & 0 & 0 & 0 & 0 \\ D & G & P & V & 0 & 0 & 0 & 0 \end{pmatrix} \end{array} \tag{B.7}$$

where

$$A = \frac{1 + e^{i(\frac{a}{2}\overrightarrow{k_2} - \frac{c}{2}\overrightarrow{k_3})} + e^{i(-\frac{a}{2}\overrightarrow{k_2} - \frac{c}{2}\overrightarrow{k_3})} + e^{i(-\frac{a}{2}\overrightarrow{k_2} + \frac{c}{2}\overrightarrow{k_3})}}{4}; \tag{B.8}$$

$$B = \frac{1 + e^{i(\frac{a}{2}\overrightarrow{k_1} + \frac{c}{2}\overrightarrow{k_3})} + e^{i(\frac{a}{2}\overrightarrow{k_1} - \frac{c}{2}\overrightarrow{k_3})} + e^{i(-\frac{a}{2}\overrightarrow{k_1} - \frac{c}{2}\overrightarrow{k_3})}}{4}; \tag{B.9}$$

$$C = e^{i(-\frac{a}{4}\overrightarrow{k_1} - \frac{a}{4}\overrightarrow{k_2})}; \tag{B.10}$$

$$D = e^{i(\frac{a}{4}\overrightarrow{k_1} - \frac{a}{4}\overrightarrow{k_2})}; \tag{B.11}$$

$$E = \frac{1 + e^{i(\frac{a}{2}\overrightarrow{k_1} - \frac{c}{2}\overrightarrow{k_3})} + e^{i(-\frac{a}{2}\overrightarrow{k_1} - \frac{c}{2}\overrightarrow{k_3})} + e^{i(-\frac{a}{2}\overrightarrow{k_1} + \frac{c}{2}\overrightarrow{k_3})}}{4}; \tag{B.12}$$

$$F = \frac{1 + e^{i(\frac{a}{2}\overrightarrow{k_2} + \frac{c}{2}\overrightarrow{k_3})} + e^{i(\frac{a}{2}\overrightarrow{k_2} - \frac{c}{2}\overrightarrow{k_3})} + e^{i(-\frac{a}{2}\overrightarrow{k_2} - \frac{c}{2}\overrightarrow{k_3})}}{4}; \tag{B.13}$$

$$G = e^{i(-\frac{a}{4}\overrightarrow{k_1} + \frac{a}{4}\overrightarrow{k_3})}; \tag{B.14}$$

$$H = \frac{1 + e^{i(-\frac{a}{2}\overrightarrow{k_2} + \frac{c}{2}\overrightarrow{k_3})} + e^{i(\frac{a}{2}\overrightarrow{k_2} + \frac{c}{2}\overrightarrow{k_3})} + e^{i(\frac{a}{2}\overrightarrow{k_2} - \frac{c}{2}\overrightarrow{k_3})}}{4}; \tag{B.15}$$

$$I = \frac{1 + e^{i(-\frac{a}{2}\overrightarrow{k_1} + \frac{c}{2}\overrightarrow{k_3})} + e^{i(\frac{a}{2}\overrightarrow{k_1} + \frac{c}{2}\overrightarrow{k_3})} + e^{i(+\frac{a}{2}\overrightarrow{k_1} - \frac{c}{2}\overrightarrow{k_3})}}{4}; \tag{B.16}$$

$$L = \frac{1 + e^{i(-\frac{a}{2}\overrightarrow{k_1} + \frac{a}{2}\overrightarrow{k_2})} + e^{i(\frac{a}{2}\overrightarrow{k_1} + \frac{a}{2}\overrightarrow{k_2})} + e^{i(\frac{a}{2}\overrightarrow{k_1} - \frac{a}{2}\overrightarrow{k_2})}}{4}; \tag{B.17}$$

$$M = \frac{1 + e^{i(-\frac{a}{4}\vec{k_1} - \frac{a}{4}\vec{k_2} + \frac{c}{2}\vec{k_3})}}{2}; \tag{B.18}$$

$$N = \frac{1 + e^{i(\frac{a}{4}\vec{k_1} - \frac{a}{4}\vec{k_2} + \frac{c}{2}\vec{k_3})}}{2}; \tag{B.19}$$

$$O = \frac{1 + e^{i(-\frac{a}{4}\vec{k_1} + \frac{a}{4}\vec{k_2} + \frac{c}{2}\vec{k_3})}}{2}; \tag{B.20}$$

$$P = \frac{1 + e^{i(\frac{a}{4}\vec{k_1} + \frac{a}{4}\vec{k_2} + \frac{c}{2}\vec{k_3})}}{2}; \tag{B.21}$$

$$Q = \frac{1 + e^{i(-\frac{a}{2}\vec{k_1} - \frac{c}{2}\vec{k_3})} + e^{i(-\frac{a}{2}\vec{k_1} + \frac{c}{2}\vec{k_3})} + e^{i(\frac{a}{2}\vec{k_1} + \frac{c}{2}\vec{k_3})}}{4}; \tag{B.22}$$

$$R = \frac{1 + e^{i(-\frac{a}{2}\vec{k_2} - \frac{c}{2}\vec{k_3})} + e^{i(-\frac{a}{2}\vec{k_2} + \frac{c}{2}\vec{k_3})} + e^{i(\frac{a}{2}\vec{k_2} + \frac{c}{2}\vec{k_3})}}{4}; \tag{B.23}$$

$$S = \frac{1 + e^{i(\frac{a}{2}\vec{k_1} - \frac{a}{2}\vec{k_2})} + e^{i(-\frac{a}{2}\vec{k_1} - \frac{a}{2}\vec{k_2})} + e^{i(-\frac{a}{2}\vec{k_1} + \frac{a}{2}\vec{k_2})}}{4}; \tag{B.24}$$

$$T = \frac{e^{i(-\frac{a}{4}\vec{k_1} + \frac{a}{4}\vec{k_2} + \frac{c}{2}\vec{k_3})} + e^{i(-\frac{a}{4}\vec{k_1} + \frac{a}{4}\vec{k_2} - \frac{c}{2}\vec{k_3})}}{2}; \tag{B.25}$$

$$U = \frac{e^{i(\frac{a}{4}\vec{k_1} - \frac{a}{4}\vec{k_2} + \frac{c}{2}\vec{k_3})} + e^{i(\frac{a}{4}\vec{k_1} - \frac{a}{4}\vec{k_2} - \frac{c}{2}\vec{k_3})}}{2}; \tag{B.26}$$

$$V = \frac{e^{i(-\frac{a}{4}\vec{k_1} - \frac{a}{4}\vec{k_2} + \frac{c}{2}\vec{k_3})} + e^{i(-\frac{a}{4}\vec{k_1} - \frac{a}{4}\vec{k_2} - \frac{c}{2}\vec{k_3})}}{2}; \tag{B.27}$$

$$Pp = \frac{1 + e^{i(\frac{a}{4}\vec{k_1} + \frac{a}{4}\vec{k_2} - \frac{c}{2}\vec{k_3})}}{2}; \tag{B.28}$$

$$Z = e^{i(\frac{a}{4}\vec{k_1} + \frac{a}{4}\vec{k_2})}; \tag{B.29}$$

$$X = \frac{1 + e^{i(-\frac{a}{4}\vec{k_1} + \frac{a}{4}\vec{k_2} - \frac{c}{2}\vec{k_3})}}{2}; \tag{B.30}$$

$$U = \frac{e^{i(\frac{a}{4}\vec{k_1} - \frac{a}{4}\vec{k_2} + \frac{c}{2}\vec{k_3})} + e^{i(\frac{a}{4}\vec{k_1} - \frac{a}{4}\vec{k_2} - \frac{c}{2}\vec{k_3})}}{2}; \tag{B.31}$$

$$W = \frac{1 + e^{i(\frac{a}{4}\vec{k_1} - \frac{a}{4}\vec{k_2} - \frac{c}{2}\vec{k_3})}}{2}; \tag{B.32}$$

$$Aa = \frac{e^{i(\frac{a}{4}\vec{k_1} + \frac{a}{4}\vec{k_2} + \frac{c}{2}\vec{k_3})} + e^{i(\frac{a}{4}\vec{k_1} + \frac{a}{4}\vec{k_2} - \frac{c}{2}\vec{k_3})}}{2}. \tag{B.33}$$

The propagator matrix $\underline{R}(\vec{k}, u)$ is then find using Eq. 4 and the diffusion coefficients are obtained by Eq. 5-7.

Appendix C. Diffusion coefficients of N: contribution of 2nd order transition states

Data availability Statements

Further data can be provided on requirements.

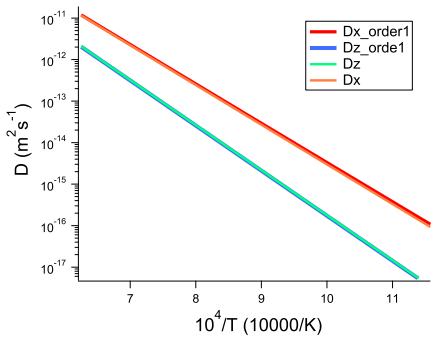

Figure C.9: Comparison of nitrogen diffusion coefficients in γ-TiAl computed including only the first order transition states (red and blue) and both the first and second order transition states (orange and green).

Acknowledgment

This work was granted access to the HPC resources of TGCC under the allocation 2019-A0060910837 attributed by GENCI (Grand Equipement National de Calcul Intensif).

References

[1] F. H. Froes, C. Suryanarayana, D. Eliezer, Synthesis, properties and applications of titanium aluminides, Journal of Materials Science 27 (19) (1992) 5113–5140.
[2] F. Appel, R. Wagner, Microstructure and deformation of two-phase gamma-titanium aluminides, Materials Science and Engineering: R: Reports 22 (5) (1998) 187–268.
[3] M. Perrut, P. Caron, M. Thomas, A. Couret, High temperature materials for aerospace applications: Ni-based superalloys and gamma-TiAl alloys, Comptes Rendus Physique 19 (8) 657–671.
[4] C. Lang, M. Schütze, TEM investigations of the early stages of TiAl oxidation, Oxidation of Metals 46 (3) (1996) 255–285.
[5] S. Becker, A. Rahmel, M. Schorr, M. Schütze, Mechanism of isothermal oxidation of the intermetallic TiAl and of TiAl alloys, Oxidation of Metals 38 (5) (1992) 425–464.
[6] S. Becker, M. Schütze, A. Rahmel, Cyclic-oxidation behavior of TiAl and of TiAl alloys, Oxidation of Metals 39 (1) 93–106.
[7] M. Schmitz-Niederau, M. Schutze, The Oxidation Behavior of Several Ti-Al Alloys at 900 C in Air, Oxidation of Metals 52 (3) (1999) 225–240.
[8] V. Shemet, A. Tyagi, J. Becker, P. Lersch, L. Singheiser, W. Quadakkers, Formation of protective alumina-based scales during high-temperature air oxidation of γ-TiAl alloys, Oxidation of Metals 54 (3) (2000) 211–235.
[9] V. Shemet, A. Tyagi, J. Penkalla, L. Singheiser, J. Becker, W. Quadakkers, Mechanisms of scale formation on new alumina forming γ-TiAl alloys studied by MCs+-SIMS, Materials at High Temperatures 17 (1) (2000) 41–47.
[10] L. Teng, D. Nakatomi, S. Seetharaman, Oxidation Behavior of TiAl-8Nb Turbine Blade Alloy, Metallurgical and Materials Transactions B 38 (3) (2007) 477–484.
[11] H. Kawaura, H. Kawahara, K. Nishino, T. Saito, New surface treatment using shot blast for improving oxidation resistance of TiAl-base alloys, Materials Science and Engineering: A 329-331 (2002) 589 – 595.
[12] H. Jiang, M. Hirohasi, Y. Lu, H. Imanari, Effect of Nb on the high temperature oxidation of Ti–(0–50 at.%)Al, Scripta Materialia 46 (9) (2002) 639 – 643.
[13] S. K. Varma, A. Chan, B. N. Mahapatra, Static and Cyclic Oxidation of Ti–44Al and Ti–44Al–xNb Alloys, Oxidation of Metals 55 (5) (2001) 423–435.
[14] M. Schütze, M. Hald, Improvement of the oxidation resistance of TiAl alloys by using the chlorine effect, Materials Science and Engineering: A 239-240 (1997) 847 – 858, 4th Conference on High-Temperature Intermetallics.
[15] N. Zheng, W. Fischer, H. Grübmeier, V. Shemet, W. Quadakkers, The significance of sub-surface depletion layer composition for the oxidation behaviour of γ-titanium aluminides, Scripta Metallurgica et Materialia 33 (1) (1995) 47 – 53.
[16] L. Niewolak, V. Shemet, C. Thomas, P. Lersch, L. Singheiser, W. Quadakkers, Oxidation behaviour of Ag-containing TiAl-based intermetallics, Intermetallics 12 (12) (2004) 1387 – 1396.
URL http://www.sciencedirect.com/science/article/pii/S0966979504001578
[17] Y. Garip, Investigation of isothermal oxidation performance of TiAl alloys sintered by different processing methods, Intermetallics 127 106985.
[18] D. Li, G. Zhang, G. Lu, J. Wang, C. Liu, Optimizing high-temperature oxidation behaviors of high-nb-containing TiAl alloys by addition of boron, Corrosion Science 177 108971.

[19] Y. Pan, X. Lu, M. D. Hayat, F. Yang, C. Liu, Y. Li, X. Li, W. Xu, X. Qu, P. Cao, Effect of sn addition on the high-temperature oxidation behavior of high nb-containing TiAl alloys, Corrosion Science 166 108449.

[20] D. O. Panov, V. S. Sokolovsky, N. D. Stepanov, S. V. Zherebtsov, P. V. Panin, N. A. Nochovnaya, G. A. Salishchev, Oxidation resistance and thermal stability of a -solidified -TiAl based alloy after nitrogen ion implantation, Corrosion Science 177 109003.

[21] J. Małecka, Transformation and precipitation processes in a metal substrate of oxidized TiAl-based alloys, Oxidation of Metals 91 (3) 365–380.

[22] C. Herzig, T. Przeorski, Y. Mishin, Self-diffusion in gamma-TiAl: an experimental study and atomistic calculations, Intermetallics 7 (3) 389–404.

[23] C. Herzig, M. Friesel, D. Derdau, S. V. Divinski, Tracer diffusion behavior of ga as an al-substituting element in ti3al and TiAl intermetallic compounds, Intermetallics 7 (10) 1141–1151.

[24] Y. Mishin, C. Herzig, Diffusion in the ti–al system, Acta Materialia 48 (3) 589–623.

[25] S. E. Kulkova, A. V. Bakulin, S. S. Kulkov, First-Principles Calculations of Oxygen Diffusion in Ti-Al Alloys, Latvian Journal of Physics and Technical Sciences 55 (6) (2018) 20–29.

[26] E. Epifano, G. Hug, First-principle study of the solubility and diffusion of oxygen and boron in the g-TiAl, Computational Materials Science 174 109475.

[27] D. Connétable, A. Prillieux, C. Thenot, J.-P. Monchoux, Theoretical study of oxygen insertion and diffusivity in the g-TiAl l10 system, Journal of Physics: Condensed Matter 32 (17) 175702, publisher: IOP Publishing.

[28] H. Eyring, The activated complex in chemical reactions, The Journal of Chemical Physics 3 (2) 107–115.

[29] U. Landman, M. F. Shlesinger, Stochastic theory of multistate diffusion in perfect and defective systems. I. mathematical formalism, Physical Review B 19 (12) 6207–6219.

[30] U. Landman, M. F. Shlesinger, Stochastic theory of multistate diffusion in perfect and defective systems. II. case studies, Physical Review B 19 (12) 6220–6237.

[31] D. Connetable, M. David, Diffusion of interstitial species (h and o atoms) in fcc systems (al, cu, co, ni and pd): Contribution of first and second order transition states, Journal of Alloys and Compounds 772 280–287.

[32] H. H. Wu, D. R. Trinkle, Direct diffusion through interpenetrating networks: Oxygen in titanium, Physical Review Letters 107 (4).

[33] D. Connétable, J. Huez, Andrieu, C. Mijoule, First-principles study of diffusion and interactions of vacancies and hydrogen in hcp-titanium, Journal of Physics: Condensed Matter 23 (40) 405401.

[34] L. Scotti, A. Mottura, Interstitial diffusion of o, n, and c in alpha-ti from first-principles: Analytical model and kinetic monte carlo simulations, The Journal of Chemical Physics 144 (8) 084701.

[35] E. Wimmer, W. Wolf, J. Sticht, P. Saxe, C. B. Geller, R. Najafabadi, G. A. Young, Temperature-dependent diffusion coefficients from ab initio computations: Hydrogen, deuterium, and tritium in nickel, Physical Review B 77 (13) 134305.

[36] D. Connetable, Theoretical study on hydrogen solubility and diffusivity in the gamma-TiAl l10 structure, International Journal of Hydrogen Energy 44 (23) 12215–12227. doi:10.1016/j.ijhydene.2019.03.110.
URL http://www.sciencedirect.com/science/article/pii/S0360319919311176

[37] G. Kresse, J. Hafner, *Ab initio* molecular dynamics for liquid metals, Phys. Rev. B 47 (1993) 558–561.

[38] G. Kresse, J. Furthmüller, Efficient iterative schemes for *ab initio* total-energy calculations using a plane-wave basis set, Phys. Rev. B 54 (1996) 11169–11186.
URL http://link.aps.org/doi/10.1103/PhysRevB.54.11169

[39] D. Connétable, M. David, Diffusion of interstitial species (h and o atoms) in fcc systems (al, cu, co, ni and pd): Contribution of first and second order transition states, Journal of Alloys and Compounds 772 280–287.

[40] G. Kresse, D. Joubert, From ultrasoft pseudopotentials to the projector augmented-wave method, Phys. Rev. B 59 (1999) 1758–1775.

[41] J. P. Perdew, K. Burke, M. Ernzerhof, Generalized Gradient Approximation Made Simple [Phys. Rev. Lett. 77, 3865 (1996)], Physical Review Letters 78 (7) (1997) 1396–1396.

[42] A. Togo, I. Tanaka, First principles phonon calculations in materials science, Scripta Materialia 108 1–5.

[43] W. B. Pearson, Handbook of Lattice Spacing and Structures of Metals and Alloys, Pergamon Press, 1964.

- The insertion of carbon and nitrogen atoms in several interstitial positions of the γ-TiAl phase has been studied using Density Functional Theory (DFT).
- The diffusion coefficients of carbon and nitrogen in γ-TiAl were obtained from *ab initio* calculations.
- We highlight and discuss the differences concerning the stable interstitial sites and the diffusion behavior between C, N and O (from previous works).
- The data here provided can help understanding the oxidation reactions of Ti-Al alloys.

E. Epifano : methodology, formal analysis, writing-original draft and writing-review and editing. **G. Hug:** conceptualisation, resources, supervision. **D. Connétable** : methodology, validation, writing-original draft.

Declaration of interests

☒ The authors declare that they have no known competing financial interests or personal relationships that could have appeared to influence the work reported in this paper.

☐The authors declare the following financial interests/personal relationships which may be considered as potential competing interests: